



## Topodiagnostic investigations on the sympathoexcitatory brain stem pathway using a new method of three dimensional brain stem mapping

J J Marx, G D Iannetti, A Mika-Gruettner, F Thoemke, S Fitzek, G Vucurevic, P P Urban, P Stoeter, G Crucchi and H C Hopf

*J. Neurol. Neurosurg. Psychiatry* 2004;75:250-255

---

Updated information and services can be found at:

<http://jnnp.bmjjournals.org/cgi/content/full/75/2/250>

---

*These include:*

**References**

This article cites 26 articles, 8 of which can be accessed free at:  
<http://jnnp.bmjjournals.org/cgi/content/full/75/2/250#BIBL>

2 online articles that cite this article can be accessed at:  
<http://jnnp.bmjjournals.org/cgi/content/full/75/2/250#otherarticles>

**Rapid responses**

You can respond to this article at:  
<http://jnnp.bmjjournals.org/cgi/letter-submit/75/2/250>

**Email alerting service**

Receive free email alerts when new articles cite this article - sign up in the box at the top right corner of the article

---

**Topic collections**

Articles on similar topics can be found in the following collections

[Brain stem / cerebellum](#) (2015 articles)  
[Radiology \(diagnostics\)](#) (9664 articles)  
[Radiology](#) (14615 articles)

---

**Notes**

---

To order reprints of this article go to:

<http://jnnp.bmjjournals.org/cgi/reprintform>

To subscribe to *Journal of Neurology, Neurosurgery, and Psychiatry* go to:

<http://jnnp.bmjjournals.org/subscriptions>

**PAPER**

# Topodiagnostic investigations on the sympathoexcitatory brain stem pathway using a new method of three dimensional brain stem mapping

**J J Marx, G D Iannetti, A Mika-Gruettner, F Thoemke, S Fitzek, G Vucurevic, P P Urban, P Stoeter, G Cruccu, H C Hopf**

*J Neurol Neurosurg Psychiatry* 2004;75:250–255

See end of article for authors' affiliations

Correspondence to:  
Dr Juergen J Marx,  
Department of Neurology,  
University of Mainz,  
Langenbeckstrasse 1, D-  
55101 Mainz, Germany;  
marx@neurologie.klinik.  
uni-mainz.de

Received 20 January 2003  
In revised form  
28 April 2003  
Accepted 3 May 2003

**Objectives:** To study the incompletely understood sympathoexcitatory pathway through the human brain stem, using a new method of three dimensional brain stem mapping on the basis of digitally postprocessed magnetic resonance imaging (MRI).

**Methods:** 258 consecutive patients presenting with acute signs of brain stem ischaemia underwent biplane T2 and EPI diffusion weighted MRI, with slice orientation parallel and perpendicular to a transversal slice selection of the stereotactic anatomical atlas of Schaltenbrand and Wahren, 1977. The individual slices were digitally normalised and projected onto the appropriate slices of the anatomical atlas. For correlation analysis lesions were imported into a three dimensional model of the human brain stem.

**Results:** 31 of the 258 patients had Horner's syndrome caused by acute brain stem ischaemia. Only four of the patients with Horner's syndrome had pontine infarctions, 12 had pontomedullary lesions, and 15 had medullary lesions. Correlation analysis showed significantly affected voxels in the dorsolateral medulla but not in the pons. A statistical comparison with infarct topology in patients with medullary lesions but without Horner's syndrome indicated that involvement of the medial and ventral part of affected voxels located in the ventrolateral medullary tegmentum was specific for Horner's syndrome.

**Conclusions:** Based on this first *in vivo* topodiagnostic study, the central sympathoexcitatory pathway probably descends through the dorsal pons before converging on specific generators in the ventrolateral medullary tegmentum at a level below the IX and X nerve exits.

The syndrome described by Horner in 1869 comprises partial ptosis, miosis with normal pupillary constriction in response to light, and facial hypohidrosis,<sup>1</sup> reflecting a classical lesion of the three neurone sympathoexcitatory pathway. According to electrophysiological and axoplasmatic transport studies in experimental animals, first order central axons descend from the hypothalamus through the brain stem and project to neurones in the intermediolateral horn of the spinal grey matter. Projections of these second order pre-ganglionic neurones terminate in the superior cervical ganglion, the axons of which run with the internal carotid nerve and plexus and terminate in the orbit, eyeball, and skin of the face.<sup>2–6</sup> Lesions involving any component of this pathway may result in the symptom complex described by Horner.

While numerous neuroanatomical and neurophysiological studies have focused on the peripheral pathway of the pre- and postganglionic neurones,<sup>7–11</sup> the course of the central sympathetic pathway involved in Horner's syndrome has not received as much attention. Anatomical case studies and electrophysiological investigations on the pupillodilator pathway, especially in the cat, hint at a brain stem pathway from the pontine tegmentum through the medullary tegmentum,<sup>12–14</sup> and axoplasmatic transport studies in the experimental animal suggest important brain stem relay centres in the lateral parabrachial nucleus,<sup>3,15</sup> the nucleus tractus solitarius,<sup>16,17</sup> and the ventrolateral medulla.<sup>18–22</sup> A few case reports on necropsy material<sup>14,23</sup> and the frequent finding of Horner's syndrome in patients with ischaemic Wallenberg's syndrome<sup>24</sup> suggest an involvement of the dorsolateral medulla in the human sympathoexcitatory pathway. However, though neuroradiological imaging had advanced considerably in the last decade, the exact localisation of the hypothalamospinal projections in the human is still unclear.

For functional localisation of the central sympathoexcitatory pathway in the human we used a new, recently published method of three dimensional brain stem mapping.<sup>25</sup> The technique was applied for the first time in a large cohort of prospectively recruited patients with acute ischaemic brain stem lesions. The functional mapping was based on digitally postprocessed magnetic resonance imaging (MRI) of acute ischaemic brain stem lesions in patients with and without subsequent Horner's syndrome.

## METHODS

Two hundred and fifty eight consecutive patients presenting with acute brain stem signs and symptoms underwent magnetic resonance imaging following a fixed protocol.

Approval for the study was granted by the university ethics committee, and patients gave informed consent to the procedures.

## Sweating test

A semiquantitative test of sweating was done, following the standard ninhydrin test procedure of Moberg. After cleaning and drying the skin, filter paper was pressed on to both sides of the patient's face. Test paper was stained with 1% ninhydrin on acetone base and developed by heating to 100°C. The test result was assessed when a typical orange colour developed on the unaffected side.

## MRI acquisition and postprocessing

Biplanar EPI-T2 and EPI diffusion weighted (DWI) MRI was done within 48 hours after the onset of symptoms with a 1.5 Tesla superconducting system (Magnetom Vision, Siemens, Erlangen, Germany). We used DWI-echo planar imaging (time of repetition (TR) 4000 ms; time of echo (TE) 103 ms) with separately applied diffusion gradients in the three

spatial axes ( $b = 1164 \text{ s/mm}^3$ , 128 matrix, 250 ms per slice, 20 slices, thickness 3 mm, eight measurements). Axial and sagittal high resolution T2 weighted imaging (TR 3810 ms, TE 90 ms, 256 matrix, slice thickness 3 mm) and T1 weighted imaging (TR 600 ms, TE 14 ms, 256 matrix, slice thickness 3 mm) before and after intravenous gadolinium was done as soon as patients could tolerate the more prolonged MRI procedure (median 6.5 days after the onset of symptoms). Slice orientation was parallel (sagittal sections) and perpendicular (axial sections) to the sagittal brain stem cuts of the stereotactic anatomical atlas of Schaltenbrand and Wahren.<sup>26</sup>

The area of infarction was identified independently by two neuroradiologists and one neurologist. Brain stem lesions were judged as acute ischaemia only if they showed corresponding EPI-diffusion weighted MRI hyperintensities.

Using Unix and NT workstations and software from Photoshop (Adobe Systems, San Jose, California, USA) and Photo-Paint (Corel, Ottawa, Canada) the individual slices were normalised and projected into 14 appropriate slices of the anatomical atlas. The zero point was set at the pontomesencephalic junction and the number of the given level indicates the distance from zero in millimetres in the craniocaudal direction.

We used axial slices for normalising the individual slices in plane according to their T2 weighted and T1 weighted brain stem outlines. Sagittal or coronal slices were applied for normalising in the z axis by determining the best fit of the anatomical plates with anatomical landmarks such as the fourth ventricle, or by setting the exit zones of the cranial nerves in projection to the anatomical plates. Given the

functional right-left symmetry of the brain stem, for an easier comparison all right sided lesions were flipped to the left side.

Slices where checked for possible contact of the projected lesions with anatomical structures marked in the atlas.

### Three dimensional mapping and statistics

Lesions were imported into a three dimensional brain stem model,<sup>25</sup> developed using data from topometric and stereotactic atlases.<sup>26–28</sup> The idealised three dimensional model of the brain stem is subdivided into 5268 volume elements ("voxels") ranging from  $2 \times 2 \times 2 \text{ mm}$  to  $2 \times 2 \times 4 \text{ mm}$ . Value 1 stands for a voxel certainly affected by the lesions, value 0 for a voxel certainly unaffected, with fractional values for intermediate probabilities. Each voxel was colour coded from white (no lesion) to red (lesion) with intermediate colours, and displayed at its proper location in the brain stem model, creating a three dimensional colour map of the whole lesion in the brain stem. From the three dimensional model, cross sectional slices can be extracted along any of the three main section planes and be further elaborated to smooth the boundaries.

Statistical analysis of patient groups aimed at identifying which voxels of the 5268 were significantly affected. For within-group one sample analysis, the system used Fisher's exact test. For each voxel, the statistical probabilities for a voxel affected in the patient group were calculated against a hypothetical mean value of the probability of a casual lesion, provided by the average number of brain stem voxels affected by ischaemia in our population. For two sample statistical analysis between two patient groups the Mann-Whitney U test was applied. Statistical significance was set at  $p < 0.05$ .

## RESULTS

Of the 258 consecutive patients presenting with acute signs of brain stem dysfunction, 41 showed a clinical Horner's syndrome comprising ptosis and miosis. Hypohidrosis of the face was clinically apparent or demonstrated by the ninhydrin sweating test in 21 of these patients. In 172 of the 258 patients, acute brain stem ischaemia could be identified by diffusion weighted MRI (DWI). One hundred and fifty one patients had a single infarct, while 21 had multiple acute brain stem lesions. Lesion location was mesencephalic in 10.5% of infarctions, pontomesencephalic in 12.5%, pontine in 36.2%, pontomedullary in 15%, and medullary in 25.8%. In the group of patients with Horner's syndrome, DWI disclosed an isolated ipsilateral acute ischaemic lesion in 31 of the 41 patients. Three patients with Horner's syndrome had multiple brain stem lesions which made anatomical-functional correlations impossible. In seven patients with Horner's syndrome no acute morphological brain stem lesion could be identified by MRI. These patients with a functional brain stem lesion obviously beyond the sensitivity of DWI were also not eligible for topodiagnostic investigations. Of the final 31 patients with acute Horner's syndrome and a single ipsilateral brain stem infarct, four had pure pontine ischaemia, 12 had a pontomedullary lesion, and 15 had a lesion in the medulla. Although most patients had dorso-lateral medullary infarction, the lesions in these patients were scattered along the rostral-caudal brain stem extension.

Of the final 31 patients, nine were female and 22 were male. Their mean age was 64.8 years, ranging from 26 to 87 years. Sonography and magnetic resonance angiography detected occlusion or stenosis of the vertebral artery in four patients. Twenty one patients had multiple vascular risk factors and sonography showed macroangiopathy of the internal carotid artery but no vertebral stenosis or occlusion. In six patients the aetiology of the infarct remained unclear (see table 1 for demographic and clinical patient data). The most common additional clinical sign of vertebrobasilar ischaemia was gait ataxia (26 patients). Other frequent symptoms were dysarthria (12 patients), trigeminal sensory

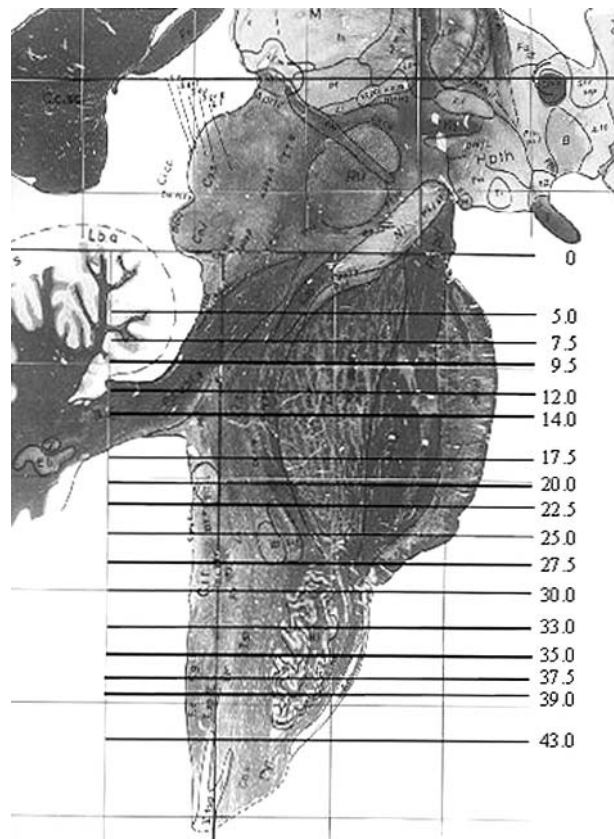


**Figure 1** Sagittal view of the brain stem showing the slices of the anatomical atlas of Schaltenbrand and Wahren<sup>26</sup> onto which the lesions have been projected. Numbers represent the distance from the pontomesencephalic junction (zero point) in millimetres in a craniocaudal direction.

**Table 1** Demographic and clinical data

Patient	Sex	Age (years)	Horner	Additional clinical signs	Lesion location
1	M	76	L	Left V nerve deficit, spontaneous nystagmus to the right, left hemiataxia, truncal and gait ataxia	Medulla
2	W	63	R	Dysarthria, emotional right facial paresis, right hemiataxia, truncal and gait ataxia	Pontomedullary
3	M	74	L	Dysarthria, right motor hemiparesis, gait ataxia	Pons
4	M	69	R	Skew deviation (lower right eye), rotatory gaze evoked nystagmus to the left, central trigeminal deficit (S1, S2), right facial palsy, dysphagia, right hemiataxia, gait ataxia	Medulla
5	M	60	L	Dysarthria, dysphagia, spontaneous nystagmus to the right, left hemiataxia, right motor hemiparesis, truncal and gait ataxia, right dissociated sensory deficit	Medulla
6	W	87	R	Dysphagia, left motor hemiparesis, right hemiataxia, gait ataxia, left dissociated sensory deficit	Medulla
7	W	72	R	Diminished right corneal reflex, right facial paresis, left dissociated sensory deficit, gait ataxia	Medulla
8	M	68	L	Dysarthria, right motor hemiparesis, gait ataxia	Pons
9	M	66	L	Left V nerve deficit, gait ataxia	Pontomesencephalic
10	W	61	L	Rotatory spontaneous nystagmus to the left, left V nerve deficit, left palate paresis, dysphagia, right dissociated sensory deficit, truncal and gait ataxia	Medulla
11	M	75	R	Right VI nerve palsy, up-beat nystagmus, gaze nystagmus to the right, right masseter paresis, right facial palsy, dysarthria, right palate paresis	Pontomedullary
12	M	67	L	Skew deviation (lower left eye), gaze nystagmus to the left, left V nerve deficit (V1), left facial palsy, dysarthria, dysphagia, truncal and gait ataxia	Medulla
13	W	68	L	Rotatory spontaneous nystagmus to the right, truncal and gait ataxia	Medulla
14	M	69	L	Skew deviation (lower left eye), left palate paresis, right dissociated sensory deficit, gait ataxia	Medulla
15	M	55	L	Left central trigeminal deficit (S1), dysphagia, dissociated sensory deficit of the right hand, gait ataxia	Medulla
16	W	77	L	Gaze evoked nystagmus to the left, left hemiataxia, right dissociated sensory deficit, gait ataxia	Medulla
17	M	69	L	Rotatory spontaneous nystagmus to the right, left facial palsy, left palate paresis, left hypoglossal paresis, dysarthria, left hemiataxia, right dissociated sensory deficit	Medulla
18	M	64	L	Left facial paresis, gaze nystagmus to the left, right motor hemiparesis, left hemiataxia, truncal and gait ataxia	Pontomedullary
19	M	69	L	Spontaneous nystagmus to the right, gait ataxia	Medulla
20	M	65	L	Gaze evoked nystagmus to the right, left V nerve deficit, left palate paresis, dysarthria, dysphagia, left hemiataxia, gait ataxia	Pontomedullary
21	M	71	L	Rotatory spontaneous nystagmus to the left, left V nerve deficit, left hypoglossal paresis, dysarthria, left hemiataxia, gait ataxia, right dissociated sensory deficit	Pontomedullary
22	M	54	R	Gaze nystagmus to the right, right palate paresis, right V nerve deficit, right facial paresis, dysarthria, truncal and gait ataxia	Medulla
23	M	51	R	Spontaneous nystagmus to the left, dysarthria, right hemiataxia, truncal and gait ataxia	Medulla
24	M	71	R	Horizontal gaze evoked nystagmus, right palate paresis, dysarthria, dysphagia, left motor hemiparesis, left dissociated sensory deficit, truncal and gait ataxia	Pontomedullary
25	W	26	R	Rotatory spontaneous nystagmus to the right, dysarthria, dysphagia, right hypoglossal paresis, right hemiataxia	Medulla
26	M	55	L	Gaze evoked nystagmus to the right, left abduction deficit, left facial palsy, right dissociated sensory deficit, right gait ataxia	Pontomedullary
27	F	65	R	Spontaneous nystagmus to the right, left motor hemiparesis, right hemiataxia, truncal and gait ataxia, left dissociated sensory deficit	Medulla
28	M	56	L	Right facial paresis, right motor hemiparesis, gait ataxia	Pontomedullary
29	M	50	L	Left V nerve deficit, right dissociated sensory deficit, gait ataxia	Medulla
30	M	74	L	Left enoral trigeminal deficit, right dissociated sensory deficit, gait ataxia	Medulla
31	F	63	L	Left hypoglossal paresis, dysarthria, right dissociated sensory deficit, left hemiataxia, gait ataxia	Medulla

F, female; L, left; M, male; R, right.

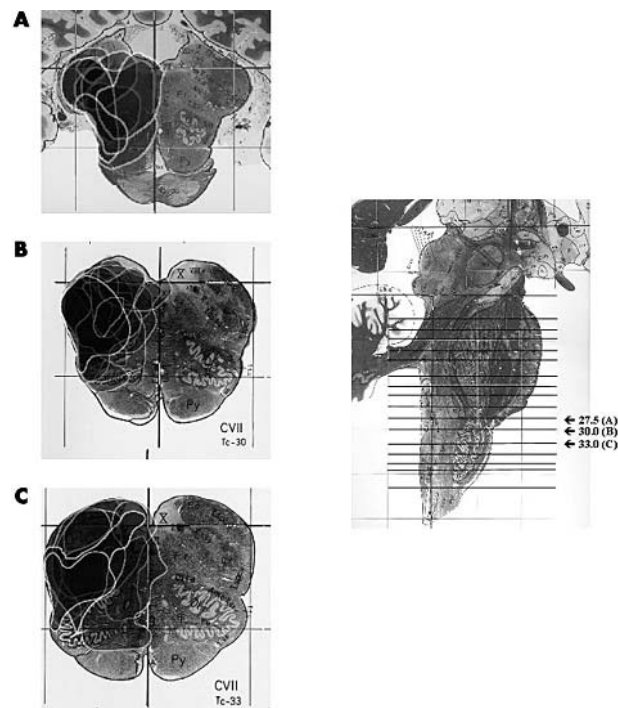


**Figure 2** Transverse atlas layers with highest density of projected lesions (27.5, 30.0, 33.0) showing the location of the lesions after superpositioning in relation to known anatomical structures. The sagittal brain stem cut shows the localisation of the transverse slices in craniocaudal extension.

disturbances (10 patients), eye movement disorders (nine patients), and hemiparesis (eight patients).

When projecting all acute brain stem lesion of these patients onto the anatomical atlas levels, the transversal slices of the atlas matching the highest number of lesions were located 27.5 to 30.0 mm caudal to the pontomesencephalic junction (fig 2).

After importing all normalised lesions into the three dimensional brain stem model, significantly affected voxels (Fisher's test:  $p < 0.05$ ) were found only in a region of the dorsal/lateral medulla (fig 3). In the craniocaudal extension, lesion maximum reached from a dorsolateral position at the pontomedullary junction to a more medial location in the lower medulla.

To ascertain which voxels were specifically related to Horner's syndrome, we selected the 16 Horner patients with medullary infarction involving the area of highest significance for further analysis. We compared the lesion topography in these 16 patients with that of the seven patients (from among the 258 initially recruited) who had an isolated infarct on the corresponding atlas levels but no clinical Horner's syndrome. Frequent associated clinical symptoms in the seven patients without Horner's syndrome but with similar lesion topography did not differ from those in the Horner group: five patients had associated gait ataxia, four suffered from dysarthria, and three had an ipsilateral trigeminal sensory deficit.

The one sample statistical analysis in the two groups of patients is shown in fig 4A and 4B. Although both groups shared many significant voxels, those of the patients with Horner's syndrome were located in a more rostral and ventral region with respect to those of the non-Horner group. The area significantly affected in the non-Horner group included the caudal and ventral part of the nucleus tractus solitarius. The two sample analysis directly comparing Horner and non-Horner patients showed that the voxels most specifically related to Horner's syndrome were located at the caudal and ventral borders of typical dorsolateral medullary infarction in

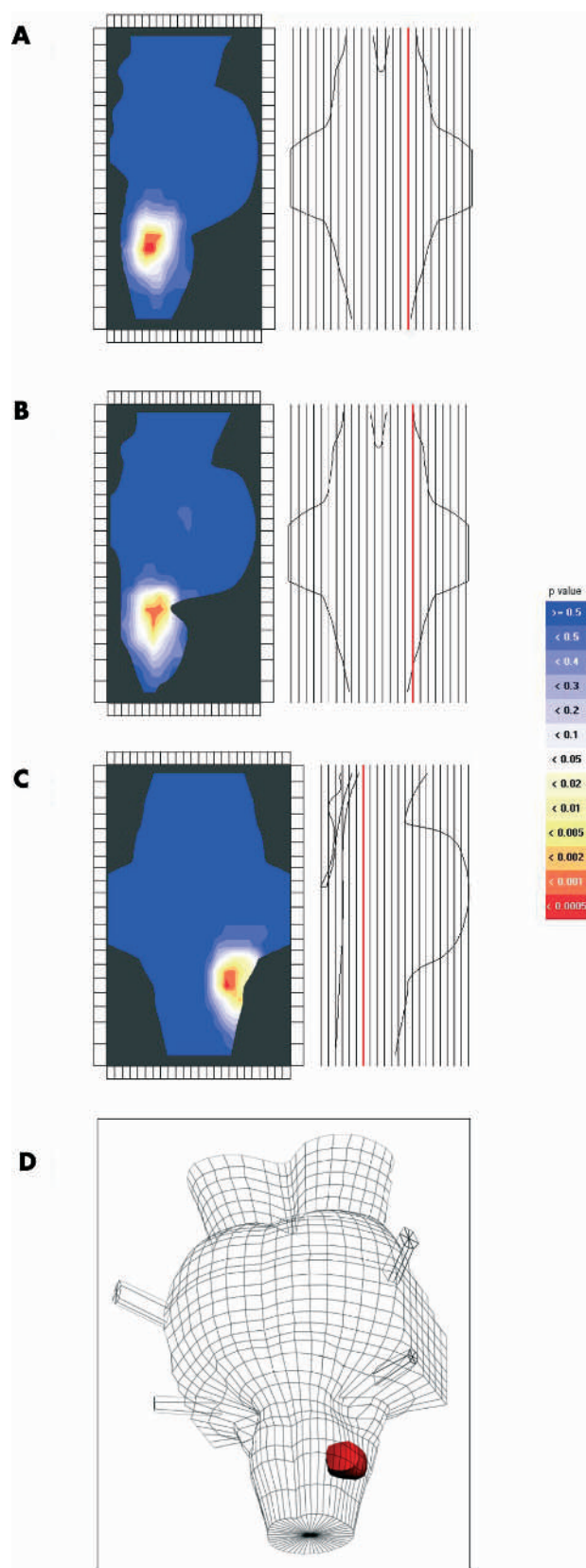


**Figure 3** Colour coded probability map of the brain stem showing significantly affected voxels in patients with Horner's syndrome in sagittal (A,B) and coronal (C) view and in a three dimensional reconstructed figure (D) on the basis of the three dimensional brain stem model by Capozza *et al*.<sup>25</sup>

the ventrolateral tegmentum of the medulla, at a level below the IX and X nerve exits (fig 4C). With respect to neighbouring anatomical structures the area was located far dorsal to the pyramidal tract, dorsal to the spinothalamic pathway through the medulla, and medial to the spinal trigeminal tract and nucleus.

## DISCUSSION

Our method is a new approach to *in vivo* brain stem mapping and allowed reliable topodiagnostic evaluation in earlier investigations.<sup>26 29 30</sup> Importing the lesions into a three dimensional brain stem model based on topometric and stereotactic atlases permits quantitative analysis with calculation of statistical probabilities and their colour coded mapping. The lesion can be studied on any plane on the three dimensional model and the relation to the central nuclei and fibre tracts examined. Spatial resolution is limited, however, by the slice thickness applied in the original scans (in this case 3 mm) and the voxel size (2×2×2 to 2×2×4 mm). Smoothing needs interpolation and may thus cause inaccuracies.

Numerous neuroanatomical and neurophysiological studies have focused on the peripheral pathways of the pre- and postganglionic neurones in patients with Horner's

syndrome,<sup>7 11</sup> probably because neuroanatomical and neurophysiological techniques were not suitable for studying the central nervous system in humans. Despite the recent progress in neuroimaging techniques, information on the central pathway involved in Horner's syndrome in man is incomplete. Occasional case reports on patients with Horner's syndrome showed MRI lesions involving the hypothalamus,<sup>24 31</sup> and Horner's syndrome has been reported in typical lateral medullary infarction<sup>24</sup> as well as in some patients with mesencephalic infarcts associated with trochlear nerve palsy.<sup>32</sup> To our knowledge no detailed topodiagnostic imaging study has been reported on the human central sympathetic pathway through the brain stem.

Despite the long craniocaudal extension of the central sympathetic pathway, in clinical experience an acute Horner's syndrome almost exclusively occurs in pontomedullary or medullary infarction and is often associated with Wallenberg's syndrome.<sup>24</sup> Consistently, our mapping analysis based on MRI postprocessing in patients with ischaemic Horner's syndrome showed that significantly affected voxels were located in the lateral medulla, in an area grossly corresponding to the infarctions produced by posterior inferior cerebellar artery occlusions. By comparing patients

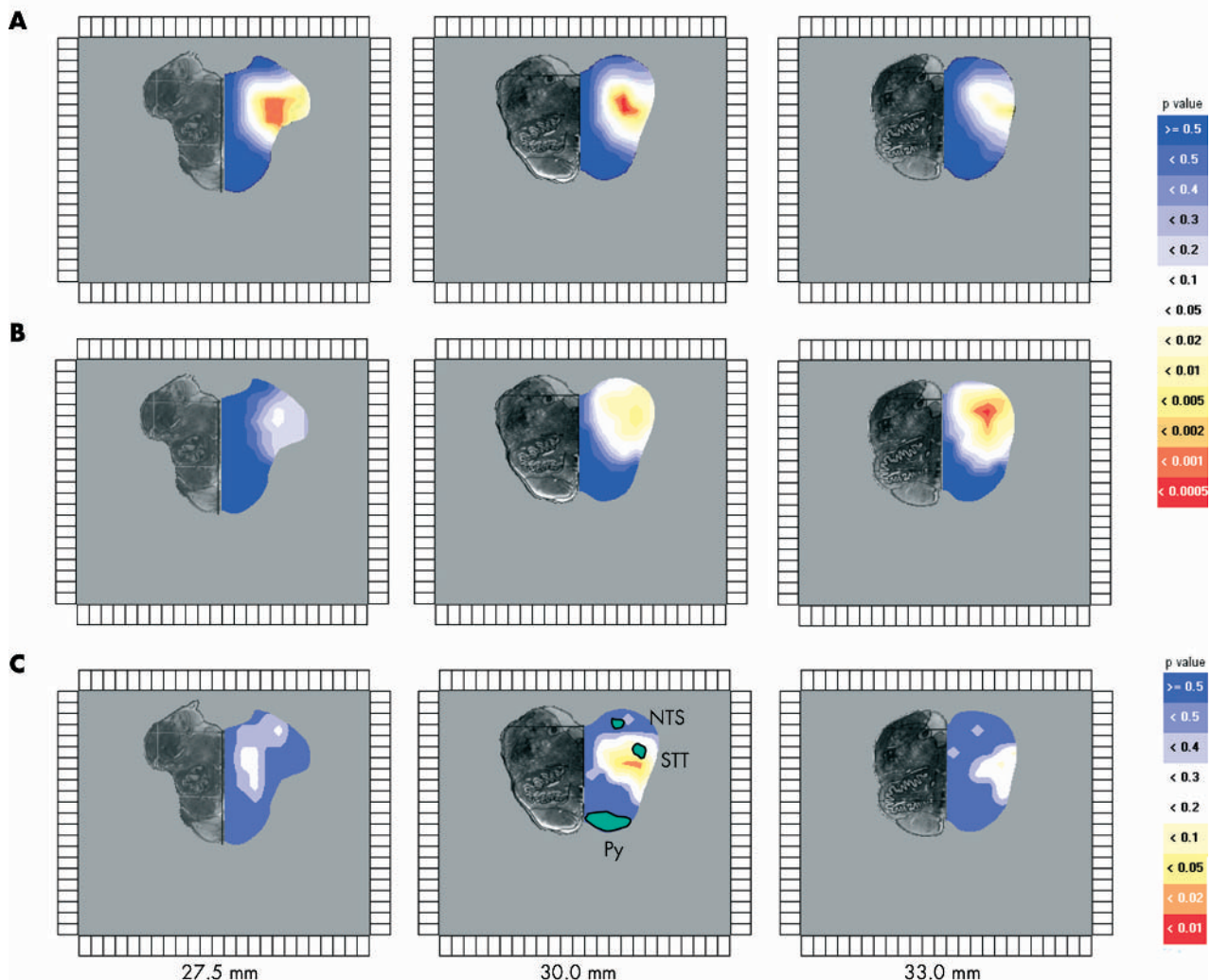


**Figure 4** (A) Colour coded probability map of axial brain stem sections showing significantly affected voxels in patients with medullary infarction plus Horner's syndrome (slice number represents the distance from the pontomesencephalic junction in craniocaudal direction in mm). (B) Same view in patients with medullary infarction but without Horner's syndrome (Fisher's exact test). (C) A two sample analysis comparing the two above groups of patients, showing the voxels specifically related to Horner's syndrome (Man-Whitney U test). On slice 30.0 the nucleus tractus solitarius (NTS), the spinal trigeminal tract (STT), and the pyramidal tract (Py) are marked in green.

with and without Horner's syndrome who had lesions at the same medullary levels (27.5, 30.0, and 33.0 mm caudal to the pontomesencephalic junction on the anatomical atlas) we could rule out the possibility that the statistical significance purely reflected the susceptibility to ischaemic damage in that vascular territory. Our analysis showed that a crucial area of the central sympathetic pathway is located in the ventrolateral medullary tegmentum at a level below the IX and X nerve exits. The area grossly corresponds to an adrenergic cell group localised in tyrosine hydroxylase tracing studies in human necropsy material, that largely contributes to the descending sympathoexcitatory pathway.<sup>14</sup>

When considering neighbouring anatomical structures and their craniocaudal extension, the area of greatest significance was located far dorsal to the pyramidal tract and to the spinothalamic pathway through the medulla, and slightly medial to the spinal trigeminal tract and nucleus. The medullary structures specifically responsible for the development of Horner's syndrome were in proximity but ventral to the area of the nucleus tractus solitarius (NTS), one of the sympathetic integration centres suggested by electrophysiological and axoplasmatic transport studies in the experimental animal.<sup>3–15</sup> Detailed analysis, however, showed that a dorsal area including this cell group was specifically affected in patients with medullary infarction but without Horner's syndrome. Thus a lesion of the NTS alone would not result in typical Horner's syndrome in man. It can even be speculated that the NTS may play an antagonistic role in the complex brain stem reflex circuit regulating sympathetic tone. According to experimental evidence hypothalamic projections include the pontine parabrachial nucleus and the NTS, and efferents from the parabrachial nucleus project to the NTS and ventrolateral medulla.<sup>12–17,18,20</sup> Thus, reciprocally connected sympathetic relay centres include cell groups of the insular cortex, amygdala, hypothalamus, parabrachial nucleus, NTS, and the ventrolateral tegmentum of the medulla—the area of highest vulnerability to sympathoexcitatory outflow impairment from our mapping analysis.<sup>3,15–17</sup>

Although most patients initially recruited in our study had acute ischaemia affecting the pons (63% of lesions), only four had Horner's syndrome. This suggests that the pontine route of the sympathetic descending tract is located in the dorsal pontine tegmentum, away from the more ventral areas frequently affected by pontine ischaemia. This agrees to the observation of Horner's syndrome in superior cerebellar artery occlusion<sup>33</sup> and in association with IV nerve palsy.<sup>32</sup> Alternatively, sympathetic fibres are still relatively scattered in the rostral brain stem so that minor pontine ischaemia does not reach a significant number of these fibres and thus will not cause clinical symptoms.

The present findings do not allow us to evaluate the possible role of other suspected integrating centres, such as the lateral parabrachial nucleus in the pons, and further imaging studies are needed to clarify the Horner pathway, especially in the upper brain stem. However, owing to the overrepresentation of medullary infarcts in our fairly large cohort of Horner patients this is going to be a challenging task.

#### Authors' affiliations

**J J Marx, A Mika-Gruettner, F Thoemke, P P Urban, H C Hopf,** Department of Neurology, University of Mainz, Mainz, Germany  
**G Vucurevic, P P Urban,** Department of Neuroradiology, University of Mainz

**G D Iannetti, G Crucu,** Department of Neurological Sciences, Università degli Studi di Roma "La Sapienza", Rome, Italy

**S Fitzek,** Department of Neurology, University of Jena, Jena, Germany

Competing interests: none declared

#### REFERENCES

- Horner JF. Über eine Form von Ptosis. *Klinische Monatsblätter für Augenheilkunde* 1869;7:193–8.
- Amanoo-Kuofi HS. Horner's syndrome revisited: with an update of the central pathway. *Clin Anat* 1999;12:345–61.
- Carpenter MB. *Core text of neuroanatomy*. Baltimore: Williams and Wilkins, 1985:266–79.
- Giles CI, Henderson JW. Horner's syndrome: an analysis of 216 cases. *Am J Ophthalmol* 1958;46:289–96.
- Lee AG, Hayman LA, Tang RA, et al. An imaging guide for Horner's syndrome. *Int J Neuroradiol* 1996;2:196–200.
- Maloney WF, Younge BR, Moyer NJ. Evaluation of the causes and accuracy of pharmacologic localization in Horner's syndrome. *Am J Ophthalmol* 1980;90:394–402.
- Jaffe NS. Localization of lesions causing Horner's syndrome. *Arch Ophthalmol* 1950;44:710–28.
- Petras JM, Cummins JF. Autonomic neurons in the spinal cord of the rhesus monkey: A correlation of the findings of cytoarchitectonic and sympathectomy with fiber degeneration following dorsal rhizotomy. *J Comp Neurol* 1972;146:189–218.
- Daalsgard CJ, Elvif LG. Spinal origin of preganglionic fibers projecting onto the superior cervical ganglion and inferior mesenteric ganglion of the guinea pig, as demonstrated by the horseradish peroxidase technique. *Brain Res* 1979;172:139–42.
- Gilbey MR, Peterson DF, Coote JF. Some characteristics of sympathetic preganglionic neurones in the rat. *Brain Res* 1982;241:43–8.
- Reuss S, Johnson RF, Morin LP, et al. Localization of spinal cord preganglionic neurons innervating the superior cervical ganglion in the golden hamster. *Brain Res Bull* 1989;22:289–93.
- Saper CB, Loewy AD, Swanson LW, et al. Direct hypothalamo-autonomic connections. *Brain Res* 1976;117:305–12.
- Loewy AD, Araujo JC, Kerr FW. Pupillodilator pathways in the brain stem of the cat: anatomical and electrophysiological identification of a central autonomic pathway. *Brain Res* 1973;60:65–91.
- Saper CB, Sorenini DM, German DC, et al. Medullary catecholaminergic neurons in the normal human brain and in Parkinson's disease. *Ann Neurol* 1991;29:577–84.
- Mosqueda-García R. Central autonomic regulation. In: Robertson D, Low PA, Polinsky RJ, eds. *Primer on the autonomic nervous system*. San Diego: Academic Press, 1996:3–12.
- Doroshenko NZ, Maiskii VA. Bulbar and pontine sources of catecholamine innervation of the rat spinal cord investigated by monoamine fluorescence and retrograde labeling techniques. *Neurophysiology* 1987;18:367–74.
- Spyer KM. Central nervous mechanisms contributing to cardiovascular control. *J Physiol (Lond)* 1994;474:1–49.
- Katayama Y, Warkins LR, Becker DP, et al. Non-opiate analgesia induced by carbachol microinjection into the pontine parabrachial region of the cat. *Brain Res* 1984;296:263–83.
- Lin AMY, Wang Y, Kuo JS, et al. Homocysteic acid elicits pressor responses from ventrolateral medulla and dorsomedial medulla. *Brain Res Bull* 1989;2:627–31.
- Lovick TA, Smith PR, Hilton SM. Spinally projecting neurons of the ventral medulla oblongata in the rat. *Brain Res Rev* 1984;11:27–33.
- McAllen RM. Mediation of fastigial pressor response and a somatosympathetic reflex by ventral medullary neurons in the cat. *J Physiol (Lond)* 1985;368:423–33.
- Su CK, Lin AMY, Lin RH, et al. Contribution between dorsal and ventrolateral regions of medulla oblongata in vasomotor function of cats. *Brain Res Bull* 1989;23:447–56.
- Nathan PW, Smith MC. The location of descending fibres to sympathetic neurons supplying the eye and sudomotor neurons supplying the head and neck. *J Neurol Neurosurg Psychiatry* 1986;49:187–94.
- Nagy AN, Hayman LA, Diaz-Marchan PJ, et al. Horner's syndrome due to first-order neuron lesions of the oculosympathetic pathway. *Am J Radiol* 1997;169:581–4.
- Capozza M, Iannetti GD, Mostarda M, et al. Three-dimensional mapping of brainstem functional lesions. *Med Biol Eng Comput* 2000;38:1–6.
- Schaltenbrand G, Wahnen W. *Atlas for stereotaxy of the human brain*. Stuttgart: Thieme, 1977.
- Paxinos G, Huang XF. *Atlas of the human brainstem*. San Diego: San Diego Academic Press, 1995.
- Kretschmann HJ, Weinrich W. *Neurofunctional systems – 3D reconstructions with correlated neuroimaging*. Stuttgart: Thieme, 1998.
- Fitzek S, Fitzek C, Marx J, et al. Blink reflex R2 changes in lower brain stem – an electrophysiological and MR-imaging study. *J Neurol Neurosurg Psychiatry* 1999;67:630–6.
- Marx JJ, Thoemke F, Fitzek S, et al. A new method to investigate brain stem structural-functional correlations using digital post-processing MRI – reliability in ischemic internuclear ophthalmoplegia. *Eur J Neurol* 2001;8:489–93.
- Bassetti C, Staikov IN. Hemiplegia vegetativa alterna (ipsilateral Horner's syndrome and contralateral hemihyperhidrosis) following proximal posterior cerebral artery occlusion. *Stroke* 1995;26:702–704.
- Sacco RL, Freddo L, Bello JA, et al. Wallenberg's lateral medullary syndrome. Clinical-magnetic resonance imaging correlations. *Arch Neurol* 1993;50:609–14.
- Hopf HC, Fitzek C, Marx J, et al. Isolated emotional facial paresis in pontine pathology. *Neurology* 2000;54:1217.